Electronic Supplementary Material (ESI) for Journal of Materials Chemistry A.
This journal is © The Royal Society of Chemistry 2017

Supporting Information

One-Pot Synthesis of Uniform Cu_2O-CuO-TiO_2 Hollow Nanocages and Highly Stable Lithium Storage Properties

Guangxia Wang,[a] Yongming Sui,*[a] Meina Zhang,[b] Man Xu,[a] Qingxin Zeng,[a] Chuang Liu,[a] Xinmei Liu,[a] Fei Du,*[ab] and Bo Zou*[a]

[a]State Key Laboratory of Superhard Materials, Jilin University, Changchun 130012, P. R. China

[b]Laboratory of Physics and Technology for Advanced Batteries (Ministry of Education), College of Physics, Jilin University, Changchun 130012, P. R. China

*Corresponding Author: zoubo@jlu.edu.cn; suiym@jlu.edu.cn; dufei@jlu.edu.cn;

Experiment section

Reagents

Copper sulfate pentahydrate ($CuSO_4 \cdot 5H_2O$), glucose ($C_6H_{12}O_6$), potassium sodium tartrate tetrahydrate and potassium hydroxide (KOH) purchased from Guoyao Chemical Reagent Company (Shanghai, China). Titanium fluoride (99%) was commercially available. All chemicals were used in the experiments without further purication. Deionized water was used throughout the experiments.

Preparation of pure Cu_2O Solid Truncated Octahedron (26-facet Cu_2O): solid truncated octahedral Cu_2O was synthesized by reduction a basic tartrate complex solution (Fehling's solution) with glucose.[1] Fehling's solution composed of 7 g L^{-1} of $CuSO_4 \cdot 5H_2O$, 25 g L^{-1} of potassium sodium tartrate tetrahydrate and 4.5 g L^{-1} of KOH. 0.4 mL (0.25M) glucose aqueous solution was added into 20 mL of the diluted stock Fehling's solution with water (volume ratio of Fehling solution and water was 1:9) during stirring. Then, the mixed solution was transferred into a static water bath and kept at 75 ℃ for 1 h. The resulting precipitates were centrifuged at 6000 rpm min^{-1} for 3 min, washed with water for twice, and finally dried at 60 ℃ for 6 h for further use.

Pure anatase TiO_2 crystals were fabricated by the same process without the addition of Cu_2O nanoparticles.[2,3]

Materials characterization

The composition of these products were investigated by Powder X-ray diffraction (XRD) using a rotating a MicroMax-007HF equipped with a rotating anode Cu-Kα target with multilayer optics and an imaging plate detector. The X-ray generator worked at 40KV and 30mA, and the X-ray beam size was reduced to 30μm using a pin-hole collimator.

The X-ray photoelectron spectroscope (XPS) was collected on the VG ESCALAB MKII spectrometer with an Mg Kr excitation (1253.6 eV).The morphology and element mapping images of the as-obtained samples was carried out by a Field emission scanning electron microscope (FESEM, FEI Company) operating at 18kV. STEM, STEM-element mapping, HRTEM, and SAED patterns were obtained on a JEM 2200FS with an accelerating voltage of 200 kV.

Electrochemical characterization

The electrochemical experiments of Cu_2O-CuO-TiO_2 electrodes were carried out by assembling coin-type half cells. The working electrode was composed of Cu_2O-CuO-TiO_2 active material (70 wt %), Ketjen Black (carbon ECP) conductive additive (20 wt %), carboxyl methylcellulose (CMC, 5 wt %) and styrene butadiene rubber (SBR, 5 wt %) dissolved in deionized water on a copper foil. The slurry mixture dried in vacuum at 100 ℃ for 12 h. After punched into round disks with a diameter of 10 mm, the test electrodes with a mass loading about 1.0-2.0 mg were assembled using metallic lithium as counter electrode and Celgard 2320 membranes as separators inside an Ar-filled glove box. The electrolyte was 1 M lithium hexafluorophosphate (LiPF6) dissolved in a mixture of ethylene carbonate (EC) and diethyl carbonate (DEC) with a volume ratio of 1:1. The galvonostatic charge−discharge cycling was conducted on a Land-2001A (Wuhan, China) automatic battery tester. Cyclic voltammetry (CV) and electrochemical impedance spectra (EIS) were performed on a VSP multichannel potentiostatic−galvanostatic system (Biologic, France). CV curves were recorded at a scanning rate of 0.1 mV s^{-1} from 0.01 V to 3.0 V. The EIS data was recorded from 1 MHz to 5 MHz by applying an AC voltage of 5 mV.

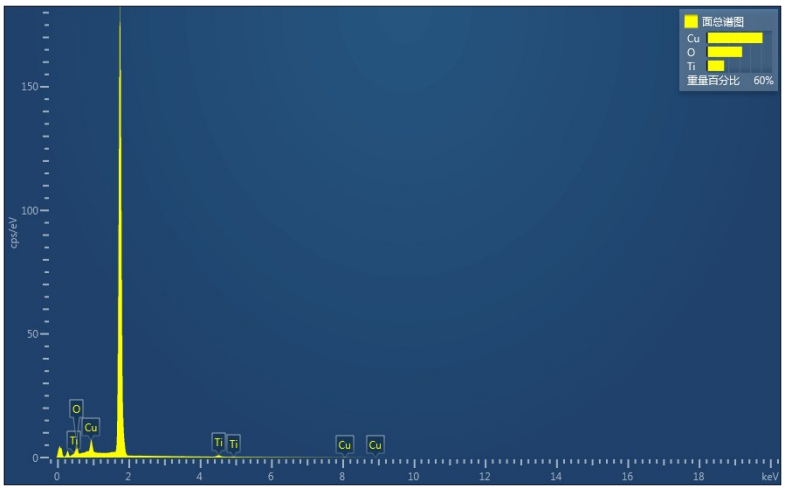

Fig. S1 Energy dispersive X-ray (EDX) spectra of Cu_2O-CuO-TiO_2.

Table S1. The composition mass ratio of Cu_2O-CuO-TiO_2 hollow nanocage in different areas. The average mass ratio of Cu and Ti is 3.4:1

Elemental/Test	1st	2nd	3rd	4th	Average
Cu	53.83	55.56	55.25	54.52	54.79
Ti	16.04	14.92	16.76	16.85	16.14

Calculation for theoretical capacities

According to the EDS analysis of composition, the element mass fraction of copper and Ti can be roughly determined as 77.2% and 22.8%, respectively. Besides, based on the XRD characterization, the relative contents of the Cu_2O phase and CuO phase in copper oxides are calculated by the height of characteristic diffraction peaks. According to $I_{Cu_2O(111)}/(I_{CuO(111)} + I_{Cu_2O(111)})$, the mass ratio of Cu_2O is about 79% in the copper oxides composites. It is noted that the mass ratio of the Cu_2O is estimated by the XRD of samples fabricated in 170 ℃ 1 h. Calculated the mass ratio between each material based on the above data, the theoretical capacity of the CCT is as follows:

$$C_{theoretical} = C_{Cu_2O} \times wt\%_{Cu_2O} + C_{CuO} \times wt\%_{CuO} + C_{TiO_2} \times wt\%_{TiO_2}$$

$$C_{CCT} = 375 \times 77.2\% \times 79\% + 674 \times 77.2\% \times 21\% + 176 \times 22.8\% = 378\ mAh\ g^{-1}$$

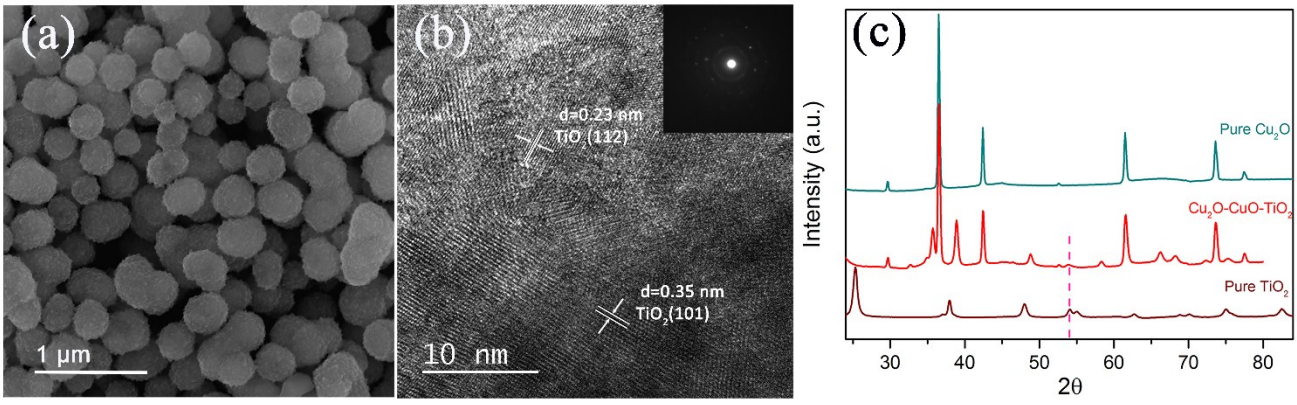

Fig. S2 (a) FESEM image and (b) HRTEM of pure TiO_2 and (c) XRD images of pure Cu_2O, Cu_2O-CuO-TiO_2 and pure TiO_2.

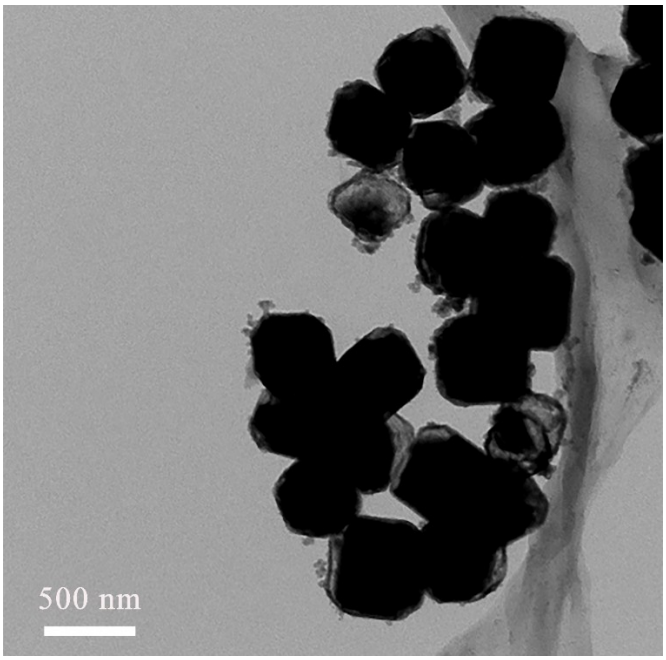

Fig. S3 STEM image of Cu_2O-CuO-TiO_2 synthesized in 170 °C for 5 min.

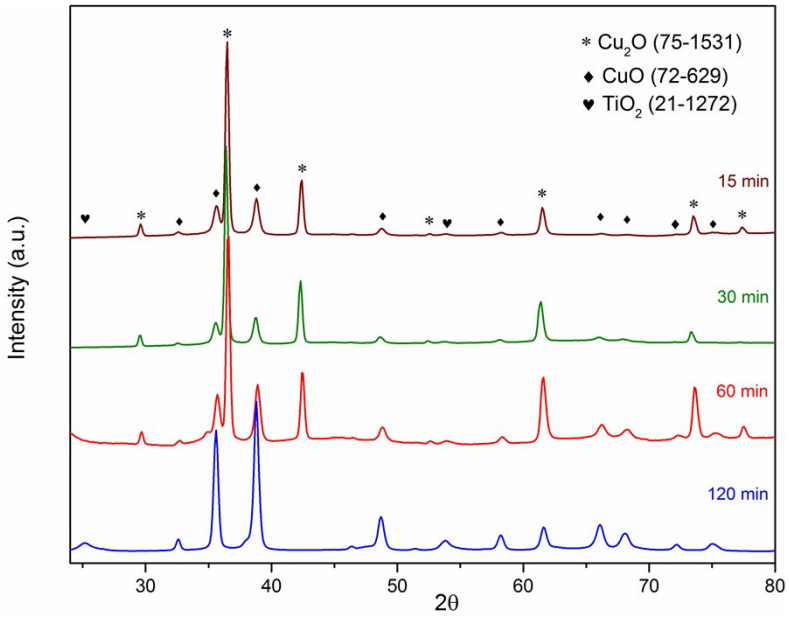

Fig. S4 XRD image of Cu_2O-CuO-TiO_2 synthesized in 170 °C for different time.

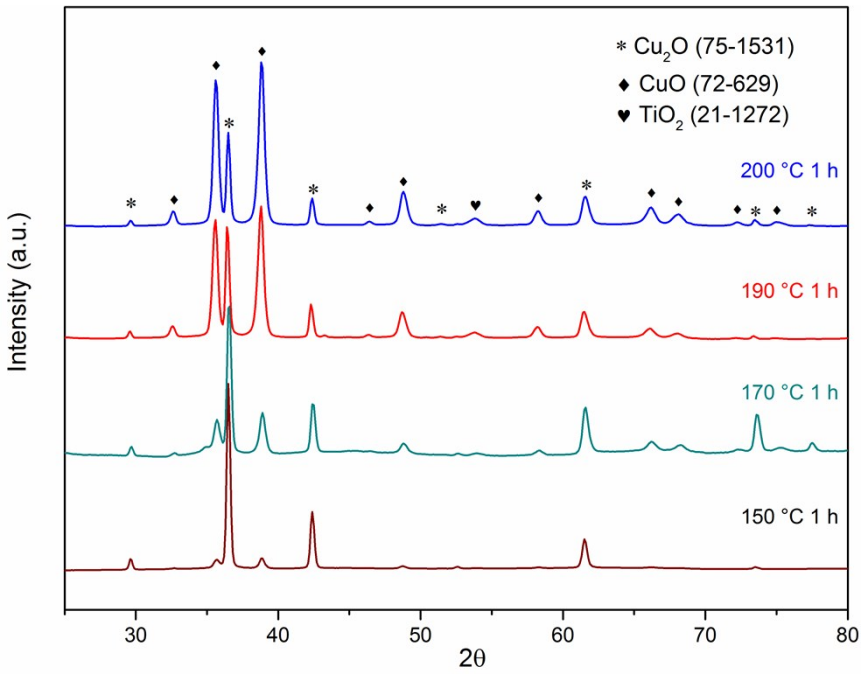

Fig. S5 XRD image of Cu_2O-CuO-TiO_2 synthesized in different temperature for 1 h.

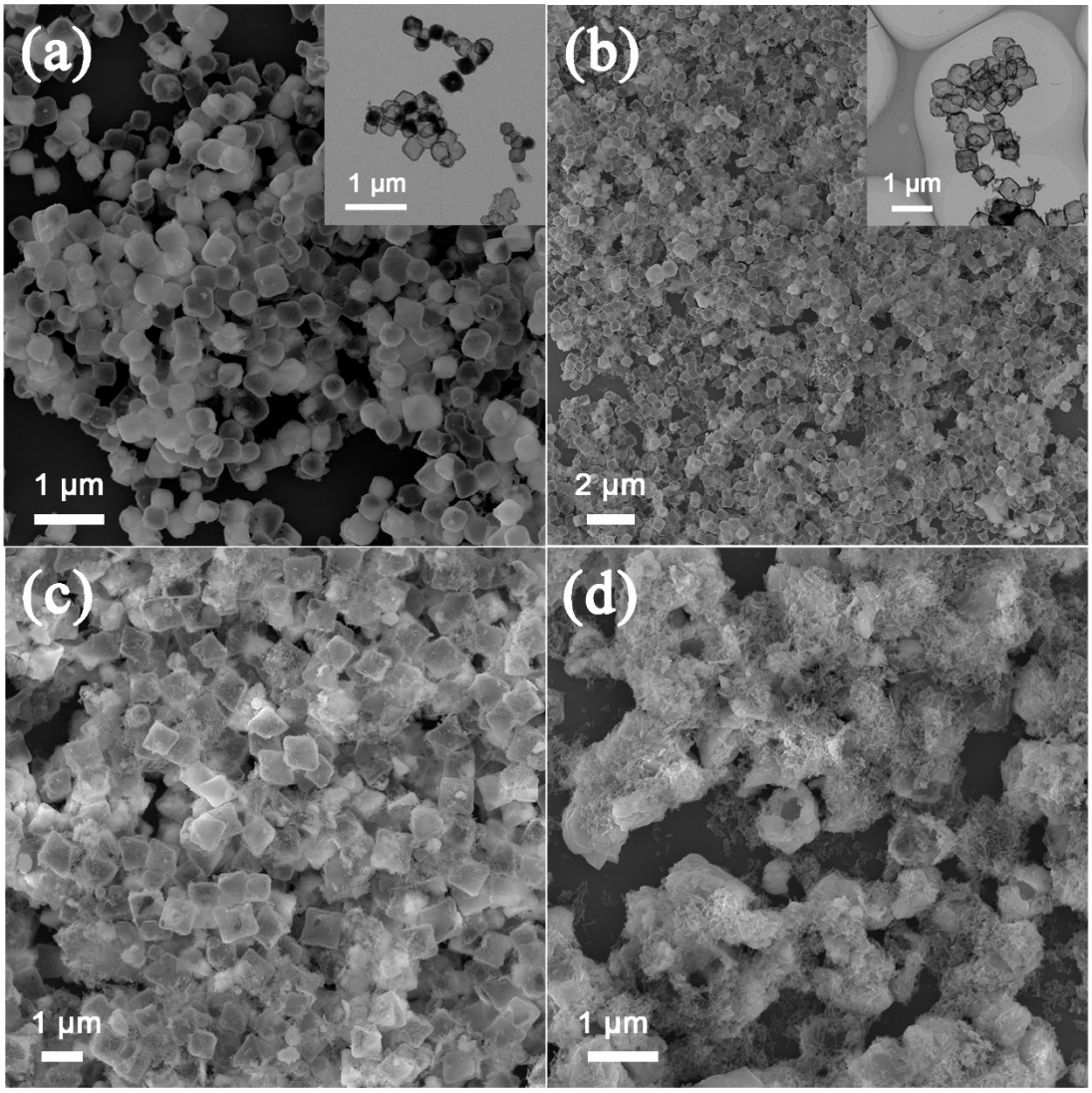

Fig. S6 FESEM images of Cu_2O-CuO-TiO_2 synthesized at (a) 160 °C and (b) 180 °C, (c) 190 °C, (d) 200 °C for 1 h.

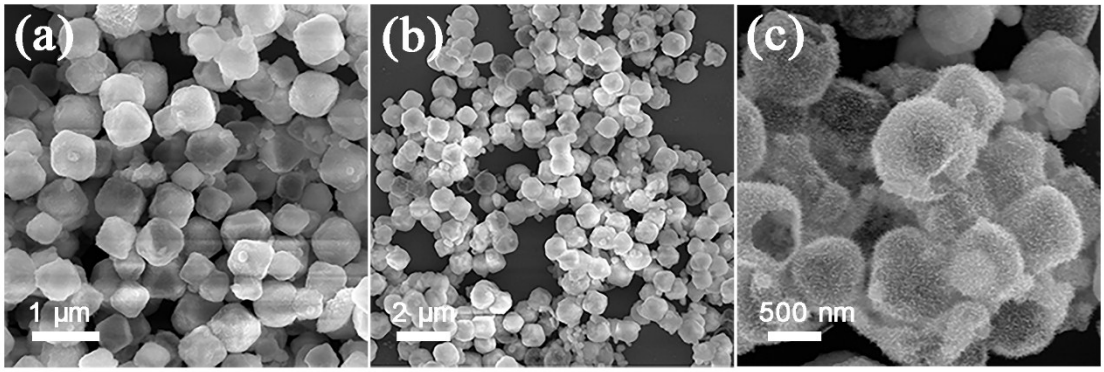

Fig. S7 FESEM images of Cu_2O-CuO-TiO_2 synthesized with different initial concentration of TiF_4 about (a) 0.64 mM, (b) 0.8 mM and (c) high magnification of 0.8 mM.

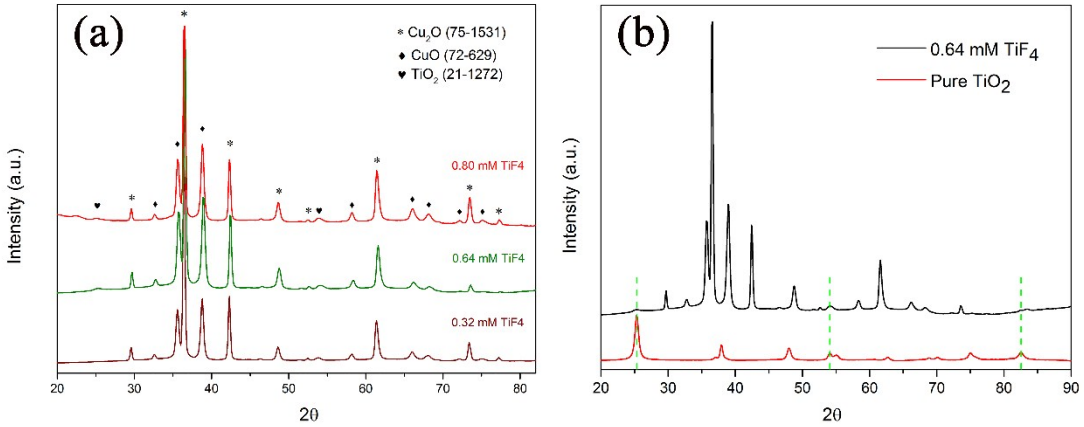

Fig. S8 XRD images of (a) Cu_2O-CuO-TiO_2 synthesized with different initial concentration of TiF_4, (b) contrast of Cu_2O-CuO-TiO_2 (initial concentration of TiF_4 is 0.64 mM) and pure TiO_2.

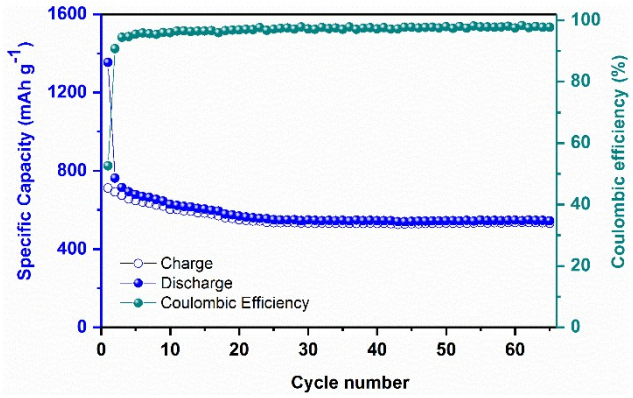

Fig. S9 The electrochemical test of Cu_2O-CuO-TiO_2 at a current density of 100 mA g^{-1}

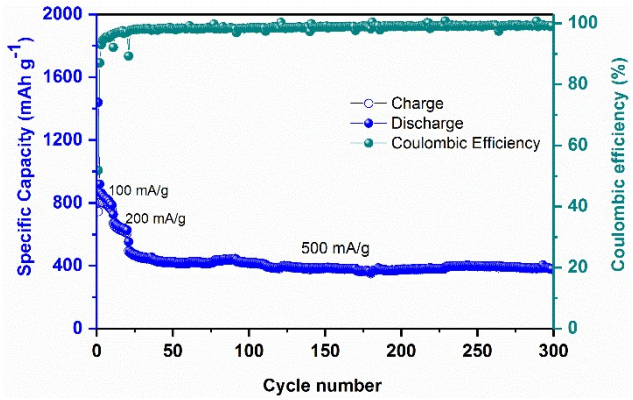

Fig. S10 Long cycling performance of Cu_2O-CuO-TiO_2 at 500 mA g^{-1}.

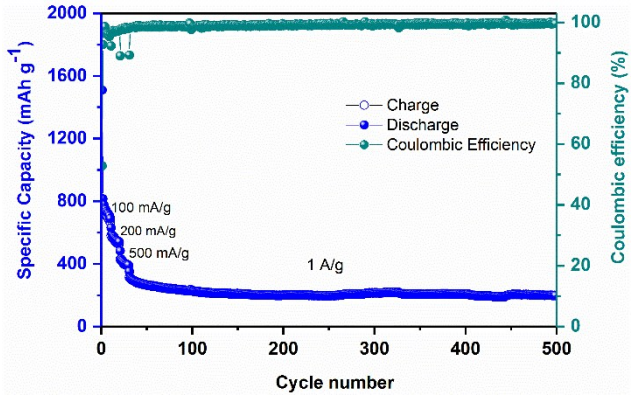

Fig. S11 Long cycling performance of Cu_2O-CuO-TiO_2 at 1 A g^{-1}.

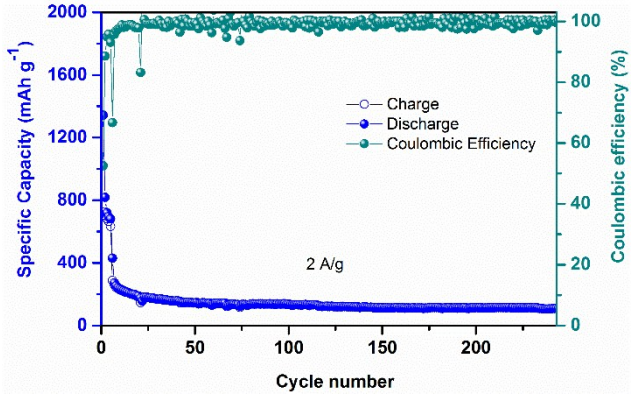

Fig. S12 Cycling performance of Cu_2O-CuO-TiO_2 at 2 A g^{-1} after activation for 5 cycles at 100 mA/g.

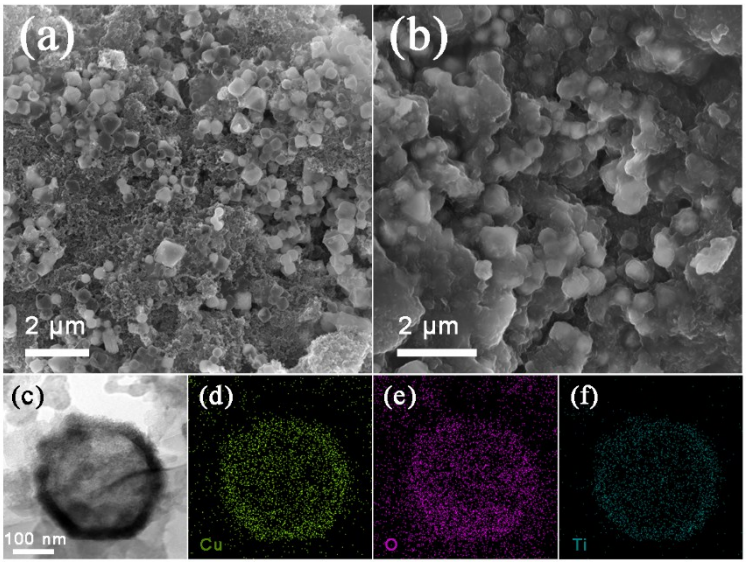

Fig. S13 FESEM images of the electrode (a) before and (b) after 100 cycles. (c-f) STEM-element mapping results of Cu, O, Ti from a single hybrid nanocage after 100 cycles.

Table S2. Electrochemical properties of hollow nanocage structured Cu_2O-CuO-TiO_2 in this work, previous reports of different structures or composite materials with Cu_2O, hollow CuO octahedra and hollow TiO_2 nanocages.

Morphology	Electrochemical properties(discharge capacity)	Current density or rate	Preparation method	Reference
Cu_2O-CuO-TiO_2 hollow nanocages	700 mAh·g^{-1}/85th cycle 546 mAh·g^{-1}/65th cycle	50 mA g^{-1} 100 mA g^{-1}	hydrothermal method	This work
26-faceted Cu_2O	145 mAh g^{-1}/50th cycle	80 mA g^{-1}	solution-phase route	4
Cu_2O with different crystal planes	397 mAh g^{-1}/50th cycle (cubes) 245.8 mAh g^{-1}/50th cycle (octahedra) 201.5 mAh g^{-1}/50th cycle (truncated octahedra)	100 mA g^{-1}	solution-phase route	5
Cu_2O nanocube	420 mAh·g^{-1}/50th cycle 236 mAh·g^{-1}/50th cycle	0.2 C 1 C	solution-phase route	6
Cu_2O hollow structure	43 mAh·g^{-1}/50th cycle (hollow octahedra) 75.3 mAh·g^{-1}/50th cycle (core@shell)	100 mA g^{-1}	solution-phase route	7
Porous Cu_2O film	336 mAh g^{-1}/50th cycle 213 mAh g^{-1}/50th cycle	0.1 C 5 C	electrodeposition	8
Cu_2O over hydrogen exfoliated graphene	430 mAh g^{-1}/25thcycle	0.1 C	deposition & heating in Ar+H_2 gas	9
Cu_2O/Ti_2CT_x (T = O, OH)	145 mAh g^{-1}/200th cycle	1000 mA g^{-1}	solvothermal method & ultrasonic treatment	10
Cu/Cu_2O/CuO heterostructures	345 mAh·g^{-1}/50th cycle	100 mA·g^{-1}	hydrothermal method & oxidation process.	11
CuO/Cu_2O hollow sphere	520 mAh·g^{-1}/20th cycle	67 mA g^{-1}	Hydrothermal method	12
CuO/Cu/TiO_2NT/Ti	226 mAh·g^{-1}/50th cycle 365 mAh·g^{-1}/50th cycle (different electrodeposition time)	_	Anodization & electrodeposition & thermal oxidation	13
CuO	429 mAh g^{-1}/50th cycle (microsphere) 392.4 mAh g^{-1}/50th cycle (flower-like) 193.0 mAh g^{-1}/50th cycle (thorn-like)	0.1 C	solution-phase route hydrothermal method	14
CuO nanofibers	426 mAh·g^{-1}/100th cycle	100 mA g^{-1}	electrospun	15

Porous CuO	320 mAh g^{-1}/50th cycle	0.1 C	hydrothermal & thermal decomposition	16
CuO hollow octahedra	470 mAh g^{-1}/100th cycle	100 mA g^{-1}	metal organic frameworks	17
CuO/C microspheres	470 mAh g^{-1}/50th cycle	100 mA g^{-1}	calcining in Ar gas followed by a oxidation treatment	18
TiO_2 nanocage	140 mAh·g^{-1}/200th cycle	0.5 C	hydrothermal method	2

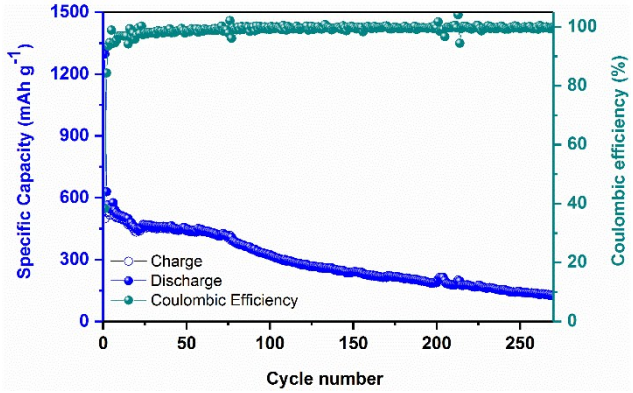

Fig. S14 Cycling performance of pure solid Cu_2O at a current density of 100 mA g^{-1}.

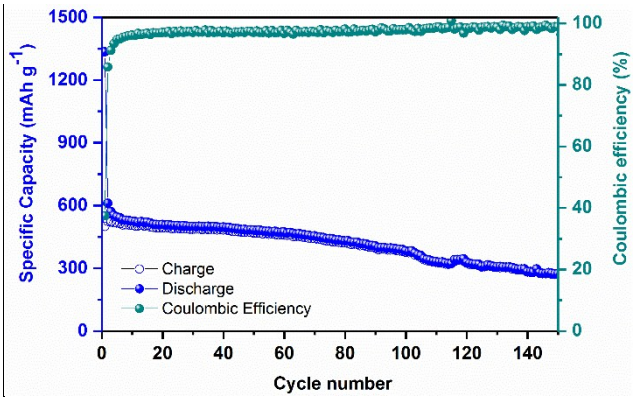

Fig. S15 Cycling performance of the nanocaged CuO at a current density of 100 mA g^{-1}.

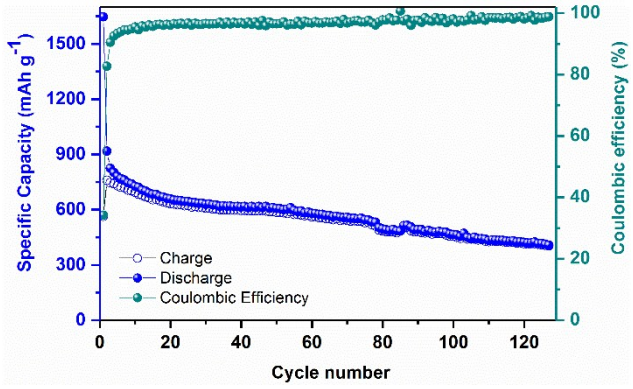

Fig. S16 Cycling performance of the rod-like solid CuO-TiO_2 at a current density of 100 mA g^{-1}.

1. C. Lu, *Adv. Mater.*, 2005, **17**(21), 2562.
2. Z. Wang and X. W. Lou, *Adv. Mater.*, 2012, **24**(30), 4124.
3. L. Liu, W. Yang, W. Sun, Q. Li and J. K. Shang, *ACS Appl. Mater. Interfaces*, 2015, **7**(3), 1465.
4. W. Kang, F. Liu, Y. Su, D. Wang and Q. Shen, *CrystEngComm*, 2011, **13**(12), 4174.
5. K. Chen, S. Song and D. Xue, *CrystEngComm*, 2015, **17**(10), 2110.
6. I. C. Chang, P.-C. Chen, M.-C. Tsai, T.-T. Chen, M.-H. Yang, H.-T. Chiu and C.-Y. Lee, *CrystEngComm*, 2013, **15**(13), 2363.
7. K. Chen, S. Song and D. Xue, *CrystEngComm*, 2013, **15**(46), 10028.
8. J. Y. Xiang, X. L. Wang, X. H. Xia, L. Zhang, Y. Zhou, S. J. Shi and J. P. Tu, *Electrochim. Acta*, 2010, **55**(17), 4921.
9. G. Ananya, N. Pranati and S. Ramaprabhu, *Int. J. Hydrogen Energy*, 2016, **41**(6), 3974.
10. H. Zhang, H. Dong, X. Zhang, Y. Xu and J. Fransaer, *Electrochim. Acta*, 2016, **202**, 24.
11. Y. Zhao, Y. Zhang, H. Zhao, X. Li, Y. Li, L. Wen, Z. Yan and Z. Huo, *Nano Res.*, 2015, **8**(8), 2763.
12. X. Guan, L. Li, G. Li, Z. Fu, J. Zheng and T. Yan, *J. Alloys Compd.*, 2011, **509**(7), 3367.
13. R. Meng, H. Hou, X. Liu, C. Yan, J. Duan and S. Liu, *Ceram. Int.*, 2016, **42**(5), 6039.
14. C. Wang, D. Higgins, F. Wang, D. Li, R. Liu, G. Xia, N. Li, Q. Li, H. Xu and G. Wu, *Nano energy*, 2014, **9**, 334.
15. R. Sahay, P. Suresh Kumar, V. Aravindan, J. Sundaramurthy, W. Chui Ling, S. G. Mhaisalkar, S. Ramakrishna and S. Madhavi, *J. Phys. Chem. C*, 2012, **116**(34), 18087.
16. M. Wan, D. Jin, R. Feng, L. Si, M. Gao and L. Yue, *Inorg. Chem. Commun.*, 2011, **14**(1), 38.
17. R. Wu, X. Qian, F. Yu, H. Liu, K. Zhou, J. Wei and Y. Huang, *J. Mater. Chem. A*, 2013, **1**(37), 11126.
18. X. H. Huang, C. B. Wang, S. Y. Zhang and F. Zhou, *Electrochim. Acta*, 2011, **56**(19), 6752.